Supporting Information

A Dual-Function Molecule Enables Stable Four-Electron Conversion and Zn Deposition for High-Capacity Aqueous Zn-I_2 Batteries

Huiquan Zhang, [a] Xueying Zhang, [a] Dongmin Ma, [a] Xinxin Cai, [a] Mochi Lv, [a] Hongting Yan, [a] Junbo Niu [b] and Weixing Song* [a]
[a]Department of Chemistry, Capital Normal University, Beijing 100048, P. R. China
E-mail: songwx@cnu.edu.cn
[b]School of Materials Science and Engineering, Nanyang Technological University, 50 Nanyang Avenue, Singapore 639798, Singapore

Experimental Section

Materials

Zinc foil (99.99%, 100 μm), titanium foil (99.99%, 30 μm) and conductive acetylene black were sourced from Shenzhen Dongxia Times Technology Company, China. Activated carbon was purchased from Xianfeng Nano. Zinc sulfate heptahydrate, L-(+)-Lysine Monohydrochloride (LLH), Carboxymethyl Cellulose (CMC), and Sodium sulfate anhydrous were purchased from Aladdin, while iodine was obtained from Macklin. Sodium chloride was purchased from Beijing Chemical Work. Glass microfiber separators (GF/D) were procured from Whatman, and all other materials were purchased from Macklin. Deionized water was used to prepare the aqueous electrolyte.

Assembly of cells: The Zn□I_2 pouch cells were configured by applying an I-containing electrode sized 1.13 cm^2 as the cathode, where Zn foil (1.13 cm^2) with a thickness of 100 μm was applied as the anode. Glass fiber discs saturated with different electrolytes (2 M $ZnSO_4$ and 2 M $ZnSO_4$ with LLH) are utilized as separators between the cathode and anode.

Fabrication of Zn||I_2 full cell: A cathode slurry was formulated by blending activated carbon, CMC, and conductive carbon black at a mass ratio of 7:2:1 in deionized water, followed by homogenization and coating onto Titanium mesh. The electrode was vacuum-dried at 60°C for 6 h. The electrode sheet was heated with I_2 at 100°C for 30 minutes, followed by excess iodine removal through heating at 40°C, synthesizing the AC/I_2 cathode.

Characterization

The morphologies of Zn foil anodes were observed by field emission scanning electron microscopy (FESEM, ZEISS Gemini 300), operated at 2 kV and 10 mA. X-ray photoelectron spectroscopy (XPS) measurements were carried out through a Thermo Scientific K-Alpha using monochromatic Al Kα radiation. The crystal structure and material composition information were gathered by X-ray diffraction (XRD, Rigaku, MiniFlex600, Cu Kα, XPS, H nuclear magnetic resonance (NMR spectroscopy (Bruker 600 MHz), and Fourier Transform Infrared Spectrometer (Thermo Scientific Nicolet iS20).

Electrochemical Measurements

All batteries were assembled in the air using pouch cells and the performances of Zn||Zn symmetric cells and Zn||I_2 full cells were collected by Land CT3002A battery test system. The electrolyte used 2 M $ZnSO_4$ in water, and all the electrodes were cut into circular pieces with a diameter of 12 mm. The stability of the zinc anode was tested using Zn||Zn cells with Glass fiber separators. In addition, non-woven fibrous membranes were used to test the cycling life under high current density. Coulombic efficiency (CE) measurements and deposition/stripping curve were performed on Zn||Ti half-cells. Electrochemical impedance spectroscopy (EIS) was carried out using a Corrtest electrochemical workstation (Corrtest, Wuhan, China) within the frequency range from 100 kHz to 0.1 Hz. Linear polarization measurements were carried out using a three-electrode system with bare Zn as the working electrode, Pt plate as the counter electrode, and Ag/AgCl as the reference electrode. Tafel curve and potentiostatic polarization were all performed on the Corrtest electrochemical workstation with a three-electrode system (Zn foil as work electrode, Pt as counter electrode, and Ag/AgCl as reference electrode).

DFT calculations

Quantum chemistry calculations were first performed to optimize molecular geometry of LLH solvent molecules, and SO_4 anions using the Gaussian 16 package [gaussian] at B3LYP/6-311+G(d,p) level of theory. The atomic partial charges on these solvent molecules and ions were calculated using the ChelpG method at the same level of theory (the B3LYP hybrid functional and the 6-311+G(d,p) basis set). The atomistic force field parameters for all ions and solvent molecules are described by the AMBER format and are taken from a previous work [amber]. The SPC/E water model was adopted in this work. The cross-interaction parameters between different atom types are obtained from the Lorentz-Berthelot combination rule.

Representative ion structures were extracted from extensive atomistic simulations, and these solvation structures were adopted as starting configurations for additional DFT calculations. DFT calculations were performed using the Gaussian 16 software [gaussian] at the same level of theory (B3LYP/6-311+G(d,p)) and with Grimme's-D3 (gd3bj) dispersion correction to obtain the corresponding optimized coordination structures and thereafter binding energies.

Additional *first principle* calculations were performed using the Vienna *ab initio* Simulation Package (VASP) [vasp]. Electron-ion interactions were described by the projector-augmented wave (PAW) pseudo potentials [potential]. The Perdew-Bruke-Ernzerh of exchange-correlation functional of the generalized-gradient approximation (GGA) was adopted, and the cutoff energy for this plane-wave basis set was set to be 450 eV, and the Γ-centered k-point grids were used for Brillouin zone integrations. The exchange-correlation functional with a Gaussian smearing width term of 0.05 eV was used. The convergence criterion for electronic self-consistent iteration was set to 1×10^{-5} eV.

The Zn (002)/(100)/(101) surfaces were constructed consisting of four atom layers. The bottom two layers in these electrodes were fixed during calculation to simulate bulk structures, while the top two atom layers were free to simulate surface state. A vacuum of 15 Å was contained in each modeling system to reduce interactions between each surface.

All structures were fully relaxed to their optimized geometries with the force convergence set to 0.01 eV/Å. The absorption of H_2O and LLH molecules on Zn (002)/(100)/(101) surfaces were comprehensively optimized to calculate the corresponding absorption energies.

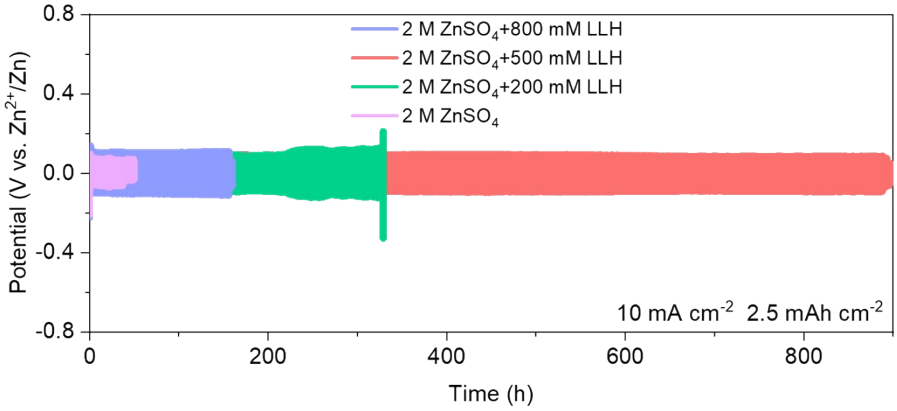

Figure S1. The electrochemical performance of Zn||Zn symmetric cells tested in $ZnSO_4$ electrolyte with different concentrations of LLH at 10 mA cm^{-2}, 2.5 mA h cm^{-2}.

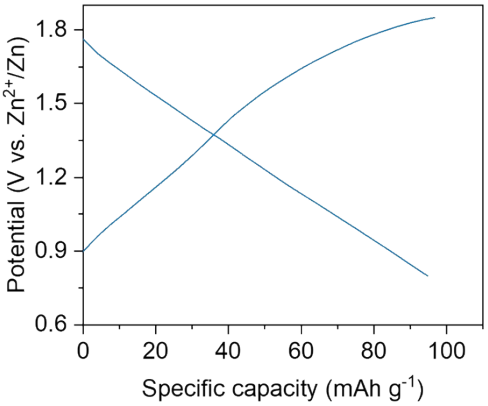

Figure S2. The discharge/charge curves of pure activated carbon.

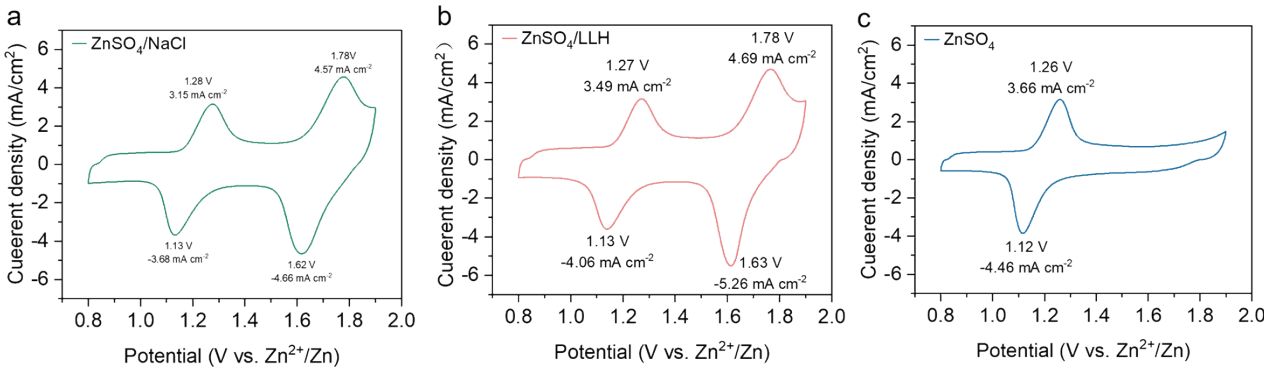

Figure S3. CV curves of different electrolytes at a scanning rate of 0.8 mV s^{-1}.

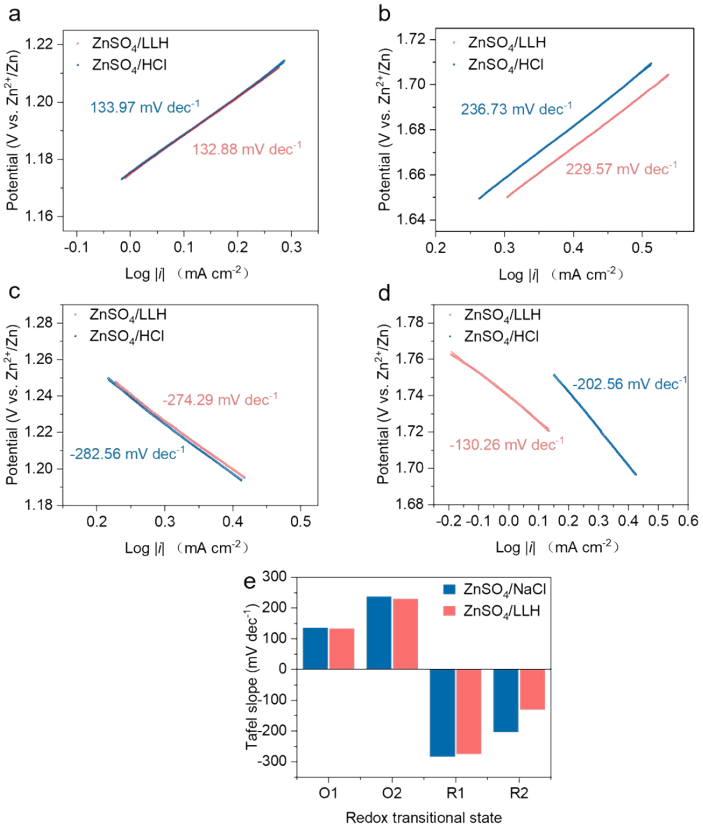

Figure S4. Reaction kinetic analysis. a, b, c, d)The Tafel slope determined from CV curves of Zn||I_2 battery. e) The conversion kinetics analysis of I_2.

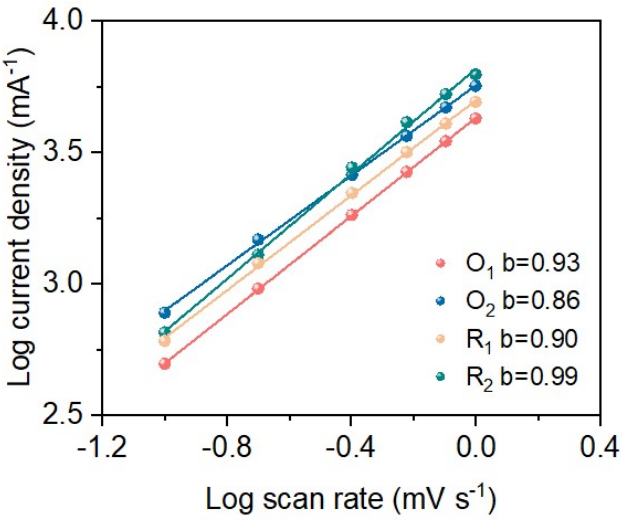

Figure S5. Plots of log i vs. log v at sharp cathodic/anodic peak pair (peak current: i_p, scan rate: v).

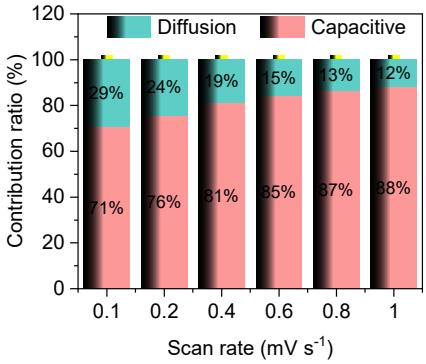

Figure S6. Proportion of surface-controlled and diffusion-controlled capacities in $ZnSO_4$ electrolytes at different scan rates.

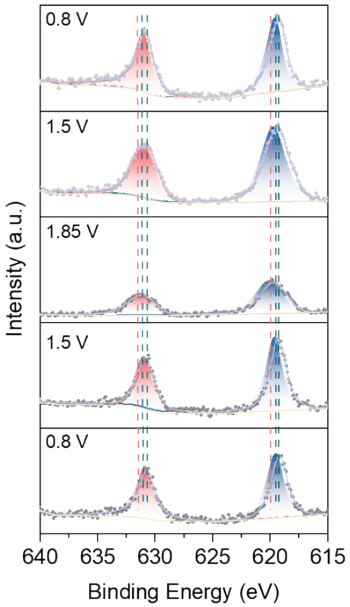

Figure S7. Ex situ XPS of I 3d at different potentials during charge and discharge.

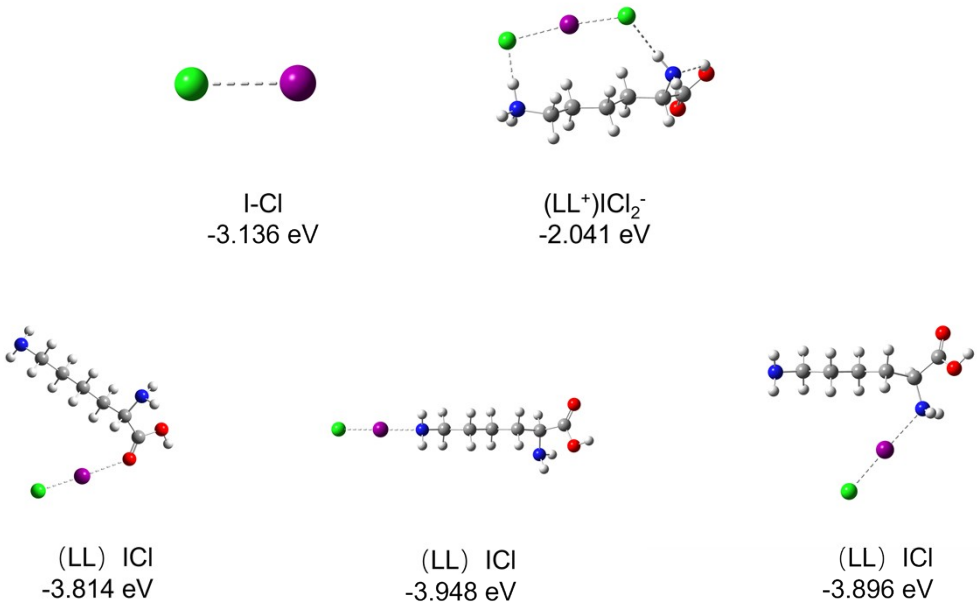

Figure S8. The different coordination forms of fixed I^+ and their binding energies.

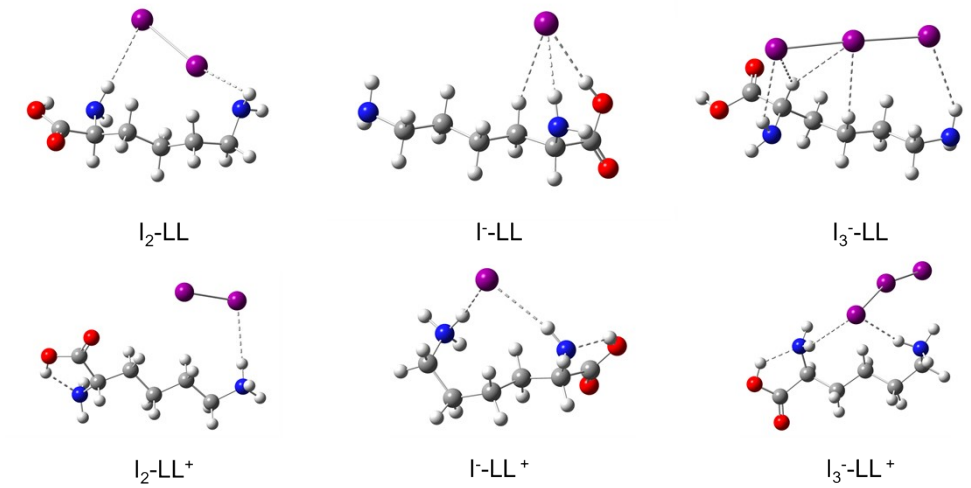

Figure S9. Binding energies of different iodine species with LL or LL $^+$.

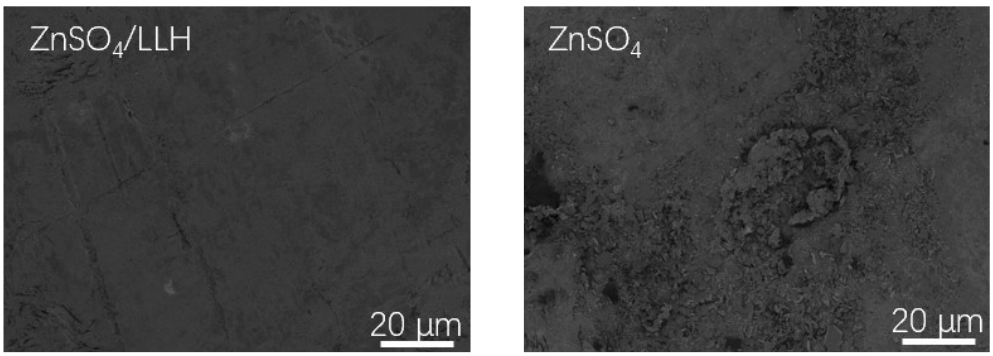

Figure S10. SEM images of Zn anode surfaces during the deposition in Zn||Zn symmetric cells at 1 mA cm^{-2}, 1 mA h cm^{-2}.

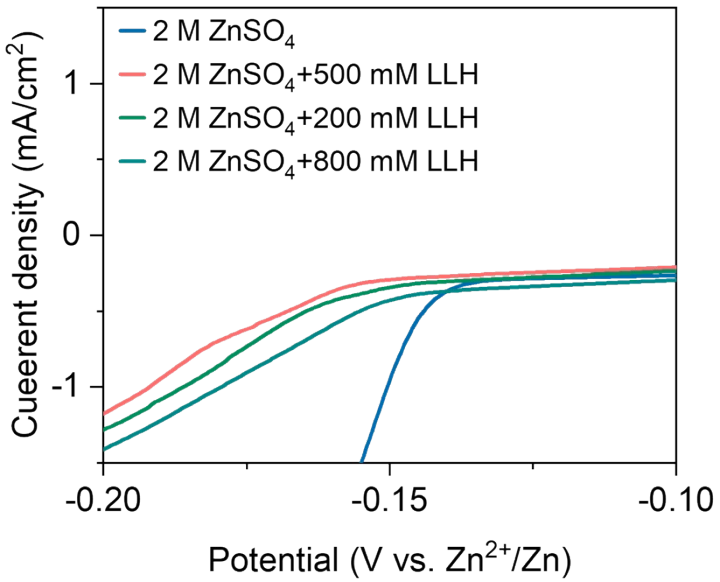

Figure S11. The linear scanning voltammetry curves of Zn||Ti cells tested at a scan rate of 1 mV s^{-1} in $ZnSO_4$ electrolyte with different concentrations of LLH.

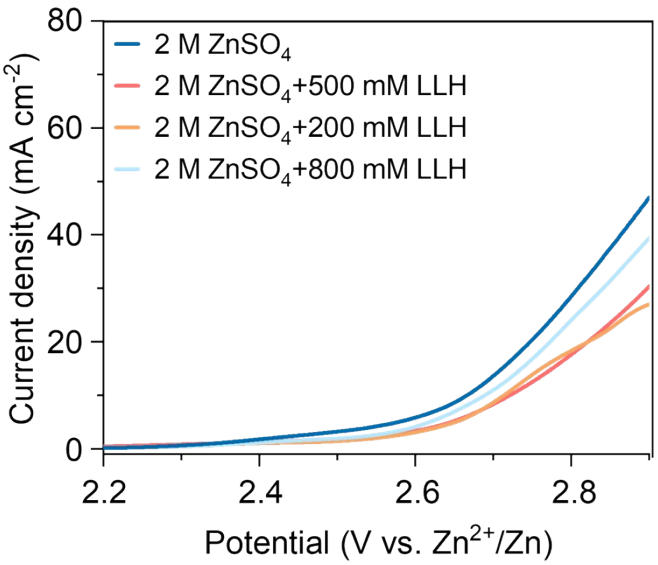

Figure S12. The H_2 evolution behaviors of Zn in $ZnSO_4$ electrolyte with different concentrations of LLH.

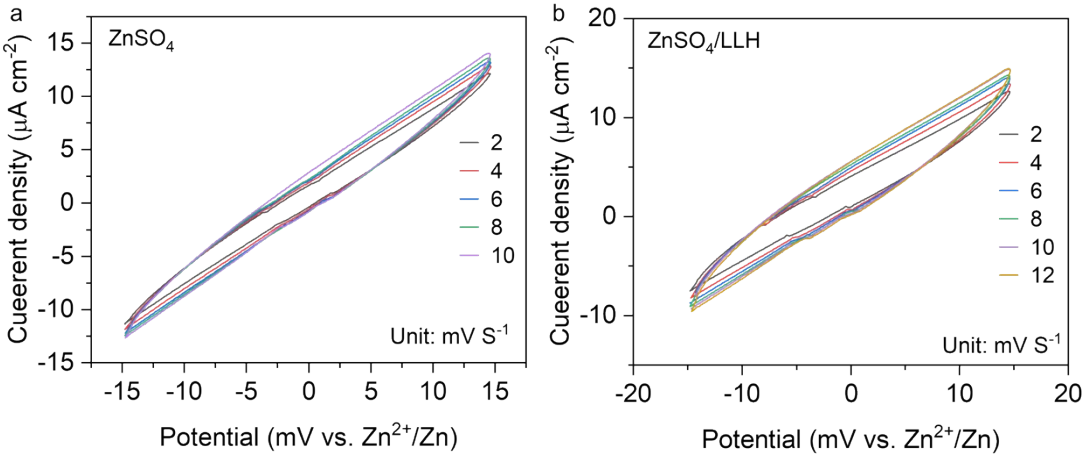

Figure S13. Electric double layer capacitance (EDLC) measurements for Zn substrates in 2 M $ZnSO_4$ electrolytes with and without LLH. The cyclic voltammetry (CV) curves for Zn||Zn cells with (a) $ZnSO_4$ electrolyte and (b) $ZnSO_4$/LLH electrolyte in a voltage range from −15 mV to 15 mV under various scanning rates.

The capacitance (C) is determined by the linear relationship between capacitive current (i_c) and scan rate (v), which can be obtained from the slope of the i_c versus v graphs. Therefore, the EDLC is calculated through the following equation:

$$c = \frac{i_c}{v}$$

Where i_c refers to the capacitive currents in CV scans. Here, we choose $i_c = (i_{0v+} - i_{0v-})/2$, meaning the half value of the current difference during forward scan and negative scan at 0 V. v refers to the scan rates of CV tests. Here, we selected 2, 4, 6, 8, and 10 mV s^{-1} as the scan rates, respectively. Corresponding CV is measured by scanning between −15 and 15 mV with Zn||Zn symmetric cells.

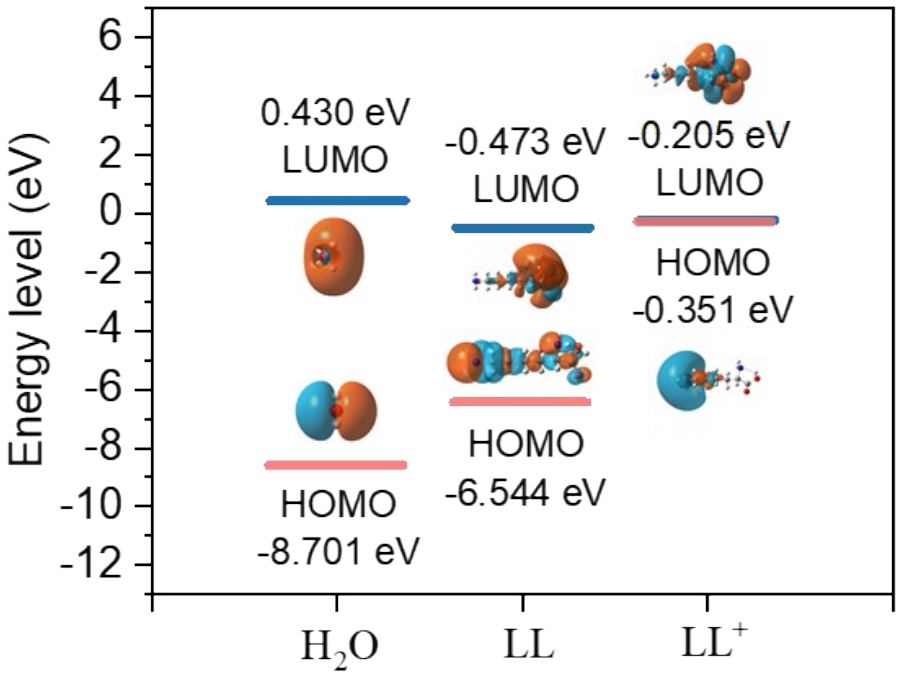

Figure S14. LUMO and HOMO energies of H_2O, LL and LL^+.

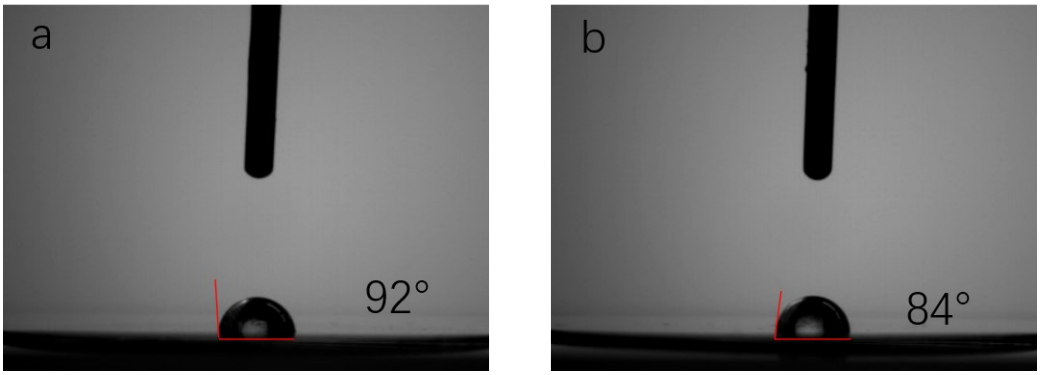

Figure S15. Contact angles of (a) $ZnSO_4$ and (b) $ZnSO_4$ with LLH on Zn foil surface.

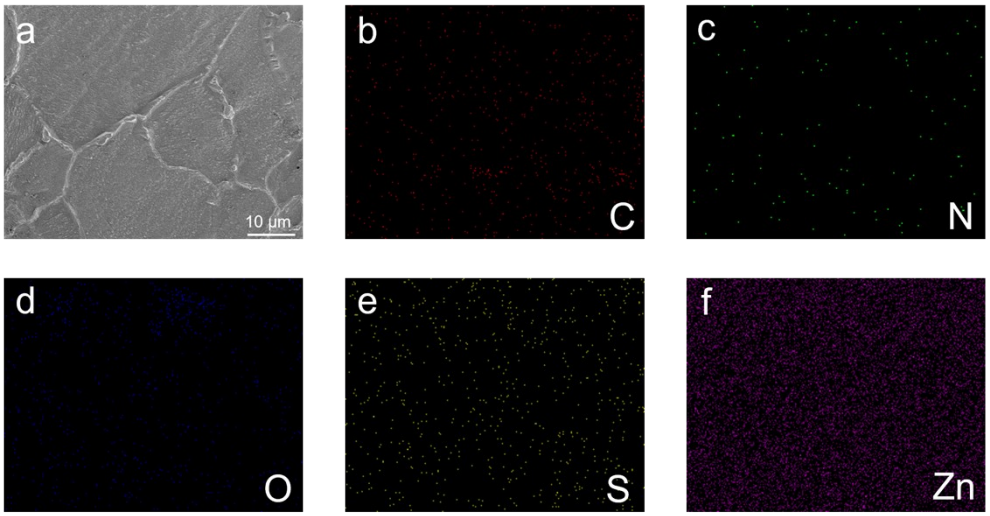

Figure S16. (a) SEM images of polished Zn after 15-day immersion in $ZnSO_4$/LLH electrolyte. The EDS mapping of (b) C, (c) N, (d) O, (e) S, (f) Zn.

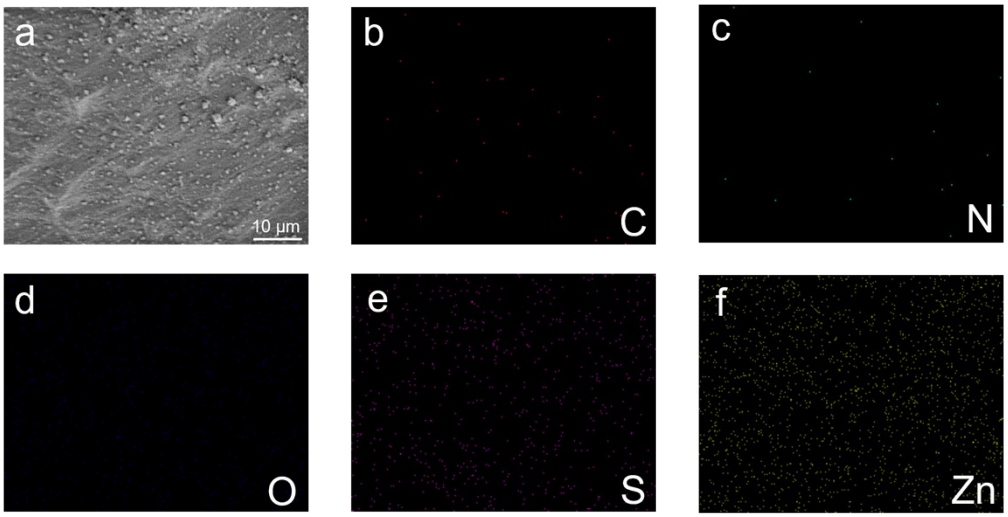

Figure S17. (a) SEM images of polished Zn after 15-day immersion in $ZnSO_4$ electrolyte. The EDS mapping of (b) C, (c) N, (d) O, (e) S, (f) Zn.

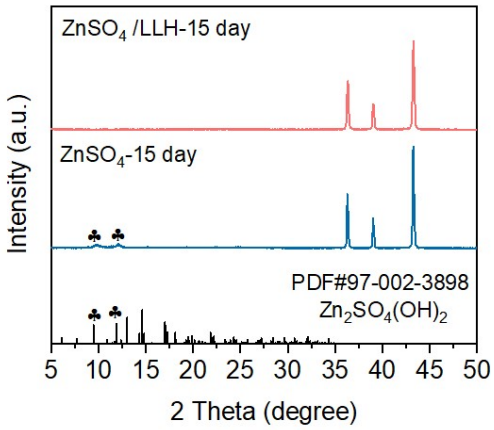

Figure S18. Corresponding XRD patterns of Zn plates after immersion in electrolytes.

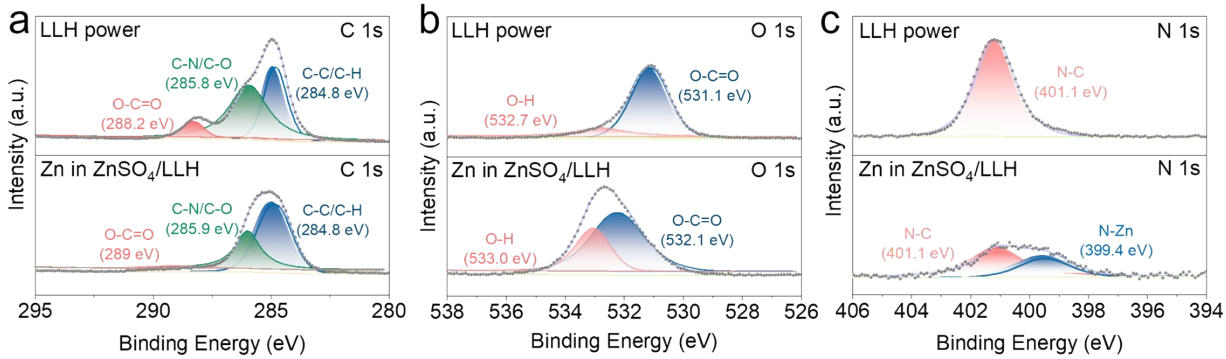

Figure S19. Zn plate after immersion in $ZnSO_4$ /LLH electrolyte and LLH powder High-resolution XPS spectra of a) C 1s, b) O 1s, and c) N 1s.

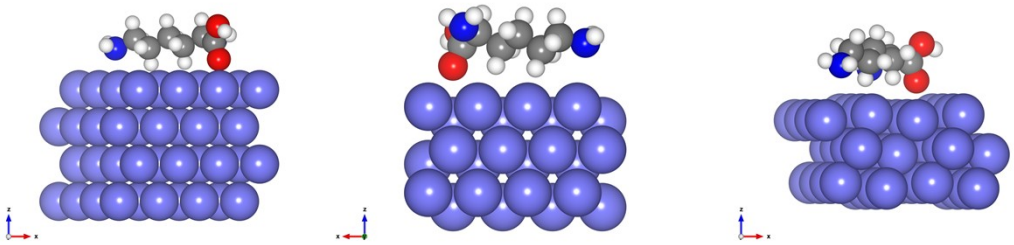

Figure S20. The optimized adsorption configurations of LL on different Zn crystal planes.

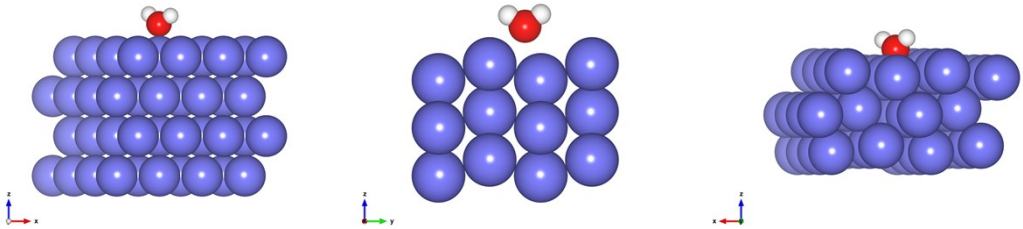

Figure S21. The optimized adsorption configurations of H_2O on different Zn crystal planes.

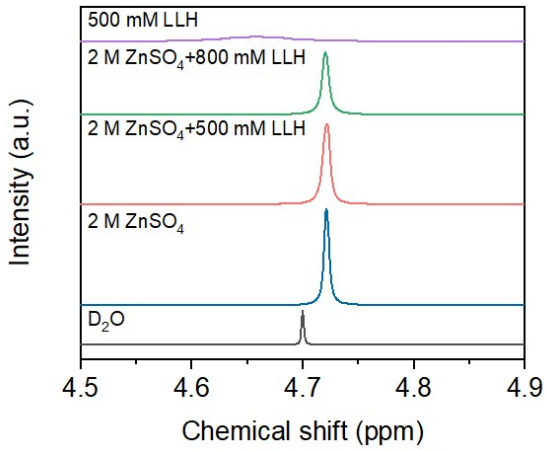

Figure S22. ^2H NMR spectra.

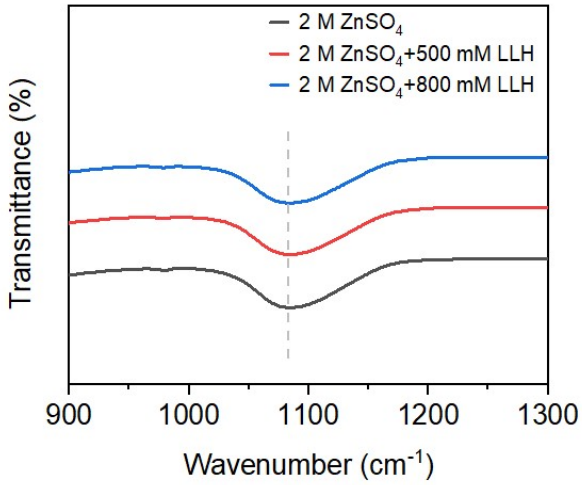

Figure S23. FTIR spectra of $ZnSO_4$ and $ZnSO_4$/LLH electrolytes.

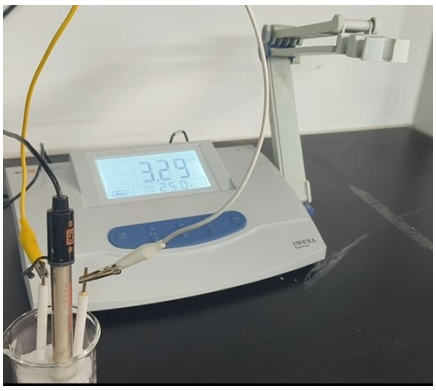

Figure S24. A digital photograph of in-situ pH detection device.

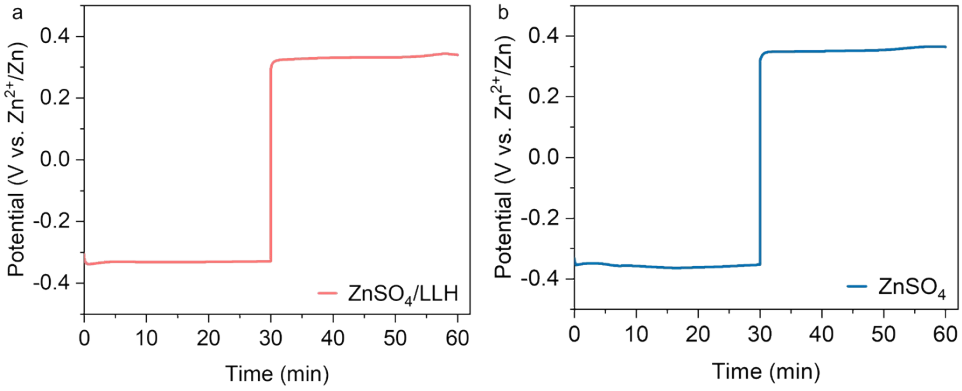

Figure S25. The electrochemical curve of Zn deposition and dissolution in the homemade in-situ pH monitoring device: a) $ZnSO_4$ /LLH, b) $ZnSO_4$.

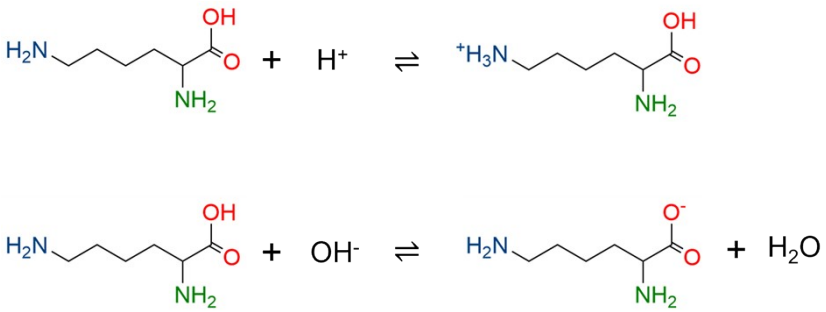

Figure S26. Proposed path for in situ pH buffer.

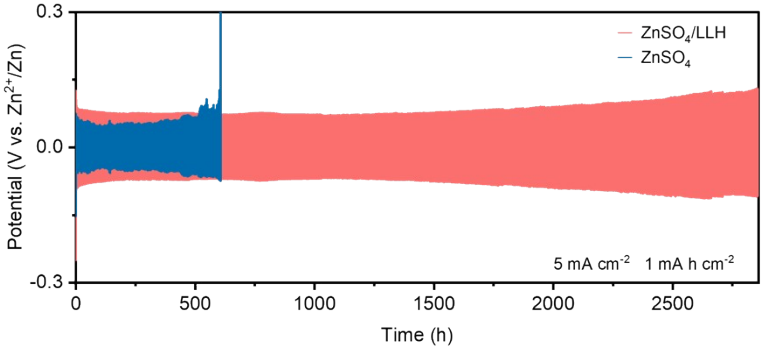

Figure S27. Galvanostatic voltage profiles of a Zn||Zn symmetric cell cycled in $ZnSO_4$ electrolytes with/without LLH for plating-stripping at 5 mA cm^{-2}, 1 mA h cm^{-2}

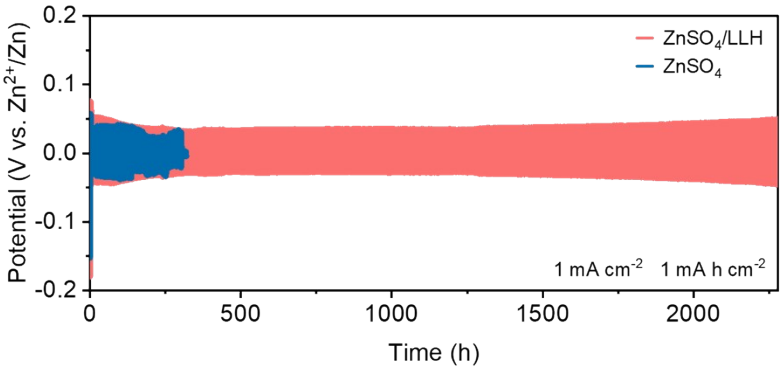

Figure S28. Galvanostatic voltage profiles of a Zn||Zn symmetric cell cycled in $ZnSO_4$ electrolytes with/without LLH for plating-stripping at 1 mA cm^{-2}, 1 mA h cm^{-2}.

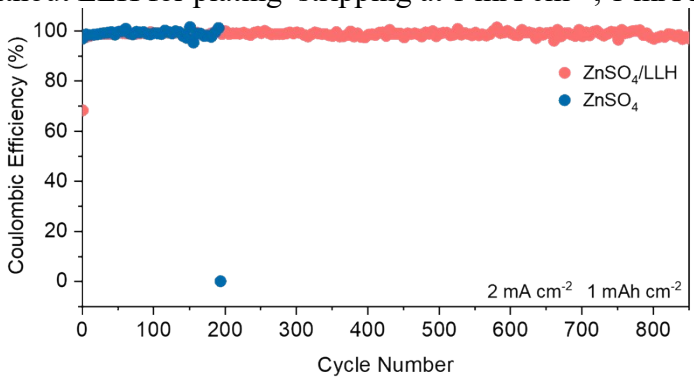

Figure S29. The CE of Zn||Ti cells in $ZnSO_4$ electrolytes with/without LLH at 2 mA cm^{-2}, 1 mA h cm^{-2}.

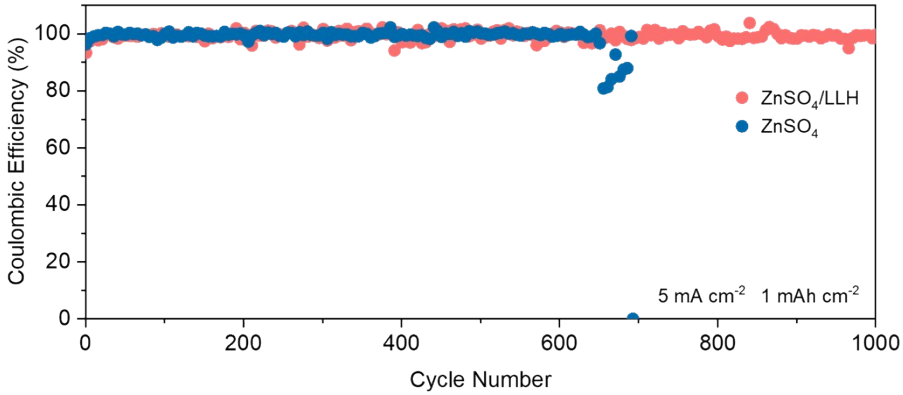

Figure S30. The CE of Zn||Ti cells in $ZnSO_4$ electrolytes with/without LLH at 5 mA cm^{-2}, 1 mA h cm^{-2}.

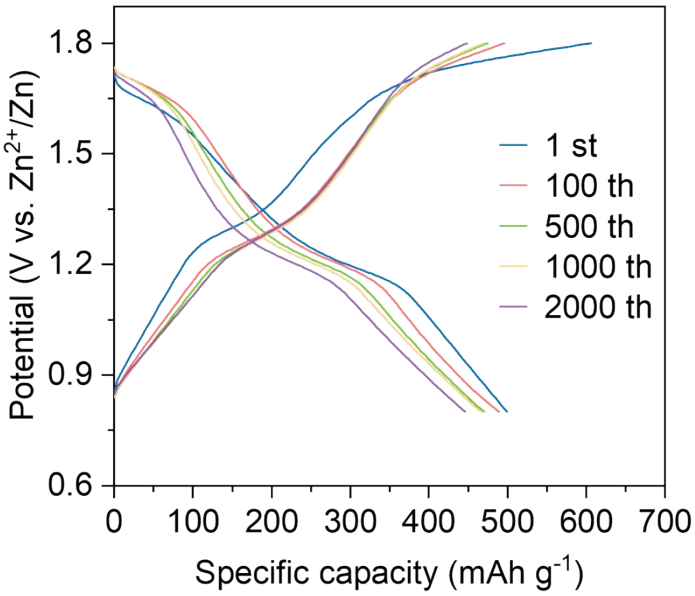

Figure S31. Galvanostatic charge–discharge curves at different numbers of cycles.

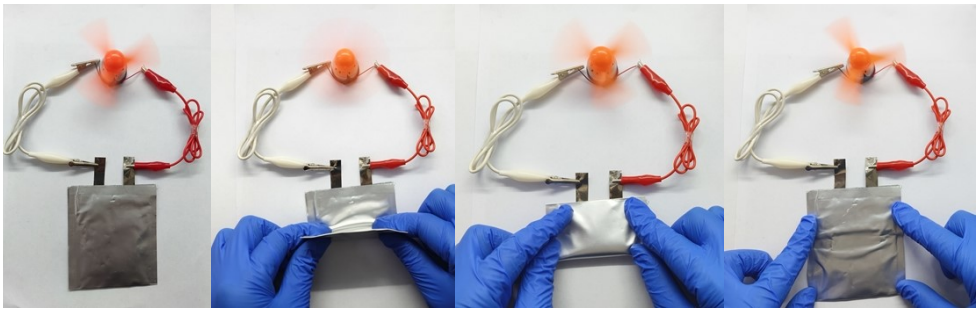

Figure S32. Pouch-type batteries folded from the initial 0° to 90°, 180°, and back to 0° for the Optical images of driving the small fan operation under different bending states.

Table S1 Comparison of electrochemical performances of four-electron-transfer-driven iodine-based batteries.

	Cathode	Electrolyte	Anode	I loading (mg cm^{-2})	Battery performance	Reference
1	$Ti_3C_2I_2$	2 M $ZnCl_2$ + 1 M KCl	Zn	1-1.5	~160 mAh·g^{-1}, 3 A g^{-1}, 2800th	[4]
2	MAI	1 M LiTFSI + 0.2 M $LiNO_3$ + 0.1 M LiCl	Li	3	408 mAh·g^{-1}, 0.5 A g^{-1}, 500th	[5]
3	AC/I_2(THA)	2 M $ZnSO_4$ + 0.5 M $N(CH_3)_3$·HCl	Zn	1	450 mAh·g^{-1}, 2 A g^{-1}, 5000th	[6]
4	BPD-HI	1 M LiTFSI + 2 wt% LiNO in DOL/DME	Li	2.5	385 mAh·g^{-1}, 2 A g^{-1}, 850th	[7]
5	Co_9S_8@NC/I_2	7.5 M $ZnCl_2$	Zn	2	415.5 mAh·g^{-1}, 5 A g^{-1}, 5000th	[8]
6	I_2@C(ZTEs)	0.5 M Niacinamide + 3 M Dimethyl sulfone + 1 M $Zn(ClO_4)_2$· $6H_2O$	Zn	1.5	395 mAh·g^{-1}, 2 A g^{-1}, 2000th	[9]
7	N/F-PC/ZnI_2	2 M $ZnSO_4$ + 0.1 M ZnI_2+0.1 M $ZnBr_2$	Zn	2	417.6 mAh·g^{-1}, 5 A g^{-1}, 8000th	[10]
8	ICu@Cu	2 M $ZnSO_4$ + 0.025 M ZnI_2	Zn	3-4	120 mAh·g^{-1}, 1 A g^{-1}, 2600th	[11]
9	$ODASnI_4$	2 M $ZnSO_4$ + 0.5 M LiCl	Zn	3	399.7 mAh·g^{-1}, 1 A g^{-1}, 2000th	[12]
	AC	2 M $ZnSO_4$ + 0.5 M LLH	Zn	1.3	416 mAh·g^{-1}, 5 A g^{-1},6000th	This work

Table S2 Comparison of prices and battery performance of different additives.

Additive	Redox type	Cycle Life	Price	Reference
LLH	$2I^-/I_2^0/2I^+$	403 mAh·g^{-1}, 5 A g^{-1}, 6000 th	¥1137.60 per 10 kg (Macklin)	This work
NaCl	$2I^-/I_2^0/2I^+$	368 mAh g^{-1}, 5 A g^{-1}, 1500 th	¥407.12 per 10 kg (Aladdin)	This work
KI	$2I^-/I_2^0$		¥7200.90 per 10 kg (Aladdin)	
Pr_4NCl	$2I^-/I_2^0/2I^+$	370 mAh g^{-1}, 5 C, 1100 th	Laboratory synthesis	[13]
N. N-bis (2-hydroxyethyl) glycine	$2I^-/I_2^0$	160 mAh g^{-1}, 2 A g^{-1}, 3000 th	¥37261 per 10 kg (Millipore)	[14]

The synthesis of quaternary ammonium salts involves complex processes and incurs high costs. Most quaternary ammonium salts reported in the literature are laboratory-synthesized and have not been produced on a large scale. Common additives such as potassium iodide or amino acids cannot simultaneously improve the performance of both the cathode and anode. While NaCl

exhibits insufficient I^+ anchoring capability at comparably low concentrations, increasing its concentration would entail higher costs and intensify side reactions.

References:

[1] M. J. Frisch, G. W. Trucks, H. B. Schlegel, G. E. Scuseria, M. A. Robb, J. R. Cheeseman, G. Scalmani, V. Barone, G. A. Petersson, H. Nakatsuji, X. Li, M. Caricato, A. V. Marenich, J. Bloino, B. G. Janesko, R. Gomperts, B. Mennucci, D. J. Hratch, Gaussian 16, Revision C.01 Gaussian, Inc., Wallingford CT **2016**.

[2] D. Chao, C. Zhu, P. Yang, X. Xia, J. Liu, J. Wang, X. Fan, S. V. Savilov, J. Lin, H. J. Fan, Z. X. Shen, *Nat. Commun.* **2016**, *7*, 12122.

[3] T. Brezesinski, J. Wang, S. H. Tolbert, B. Dunn, *Nature Mater.* **2010**, *9*, 146–151.

[4] X. Li; M. Li; Z. Huang; G. Liang; Z. Chen; Q. Yang; Q. Huang; C. Zhi, Activating the I^0/I^+ redox couple in an aqueous I_2–Zn battery to achieve a high voltage plateau. *Energy Environ. Sci.* **2021,** *14* (1), 407-413.

[5] X. Li, Y. Wang, Z. Chen, P. Li, G. Liang, Z. Huang, Q. Yang, A. Chen, H. Cui, B. Dong, H. He, C. Zhi, Two-Electron Redox Chemistry Enabled High-Performance Iodide-Ion Conversion Battery. *Angew. Chem. Int. Ed.* **2022,** (9), e202113576.

[6] M. Wang, Y. Meng, M. Sajid, Z. Xie, P. Tong, Z. Ma, K. Zhang, D. Shen, R. Luo, L. Song, L. Wu, X. Zheng, X. Li, W. Chen, Bidentate Coordination Structure Facilitates High-Voltage and High-Utilization Aqueous Zn−I_2 Batteries. *Angew. Chem. Int. Ed.* **2024,** *63* (39), e202404784.

[7] F. Zhu, Z. Li, Z. Wang, Y. Fu, W. Guo, From Inorganic to Organic Iodine: Stabilization of I^+ Enabling High-Energy Lithium–Iodine Battery. *Journal of the American Chemical Society* **2024,** *146* (16), 11193-11201.

[8] T. Hu, Y. Zhao, Y. Yang, H. Lv, R. Zhong, F. Ding, F. Mo, H. Hu, C. Zhi, G. Liang, Development of Inverse-Opal-Structured Charge-Deficient Co9S8@nitrogen-Doped-Carbon to Catalytically Enable High Energy and High Power for the Two-Electron Transfer I^+/I^- Electrode. **2024,** *36* (18), 2312246.

[9] C. Li, H. Li, X. Ren, L. Hu, J. Deng, J. Mo, X. Sun, G. Chen, X. Yu, Urea Chelation of I^+ for High-Voltage Aqueous Zinc–Iodine Batteries. *ACS Nano* **2025,** *19* (2), 2633-2640.

[10] X. Kong, J. Zhang, X. Zhang, Z. Wang, D. Wang, Boosting Reversible Four-Electron Redox in Aqueous Zn-Iodine Batteries with Two Halogen Ionic Additives and a N, F Codoped Carbon Cathode. *ACS Applied Energy Materials* **2025,** *8* (1), 601-610.

[11] X. Yang, Y. Zhang, L. Wang, J. Kang, Z. Zhai, J. Zhang, L. Zhang, H. Lu, Anode-free Zn–I_2 batteries without fear of Zn loss: Hybrid energy-storage mechanism and dynamic capacity compensation. *J. Colloid Interface Sci*. 2025, 698, 138010.

[12] X. Li, S. Wang, D. Zhang, P. Li, Z. Chen, A. Chen, Z. Huang, G. Liang, A. L. Rogach, C. Zhi, Perovskite Cathodes for Aqueous and Organic Iodine Batteries Operating Under One and Two Electrons Redox Modes. *Adv. Mater.* **2023,** *36* (4), 2304557.

[13] P. Jiang, Q. Du, C. Lei, C. Xu, T. Liu, X. He and X. Liang, Stabilized four-electron aqueous zinc–iodine batteries by quaternary ammonium complexation, Chem. Sci., 2024, 15, 3357-3364.

[14] J. Bu, P. Liu, G. Ou, M. Ye, Z. Wen, Y. Zhang, Y. Tang, X. Liu, C. Li, Interfacial Adsorption Layers Based on Amino Acid Analogues to Enable Dual Stabilization toward Long-Life Aqueous Zinc Iodine, Adv. Mater., **2025**, 202420221